

Anomalous Quadrupole Topological Insulators in 2D Nonsymmorphic Sonic Crystals

Zhi-Kang Lin,¹ Hai-Xiao Wang,^{2,1} Zhan Xiong,¹ Ming-Hui Lu,³ and Jian-Hua Jiang^{1,*}

¹*School of Physical Science and Technology, & Collaborative Innovation Center of Suzhou Nano Science and Technology, Soochow University, 1 Shizi Street, Suzhou 215006, China*

²*College of Physics and Technology, Guangxi Normal University, Guilin 541004, China*

³*National Laboratory of Solid State Microstructures and Department of Materials Science and Engineering, Nanjing University, Nanjing, 210093, China, & Collaborative Innovation Center*

of Advanced Microstructures, Nanjing University, Nanjing, 210093, China

(Dated: May 21, 2020)

The discovery of quadrupole topology opens a new horizon in the study of topological phenomena. However, the existing experimental realizations of quadrupole topological insulators in symmorphic lattices with π -fluxes often break the protective mirror symmetry. Here, we present a theory for anomalous quadrupole topological insulators in nonsymmorphic crystals without flux, using 2D sonic crystals with $p4gm$ and $p2gg$ symmetry groups as concrete examples. We reveal that the anomalous quadrupole topology is protected by two orthogonal glide symmetries in square or rectangular lattices. The distinctive features of the anomalous quadrupole topological insulators include: (i) minimal four bands below the topological band gap, (ii) nondegenerate, gapped Wannier bands and special Wannier sectors with gapped composite Wannier bands, (iii) quantized Wannier band polarizations in these Wannier sectors. Remarkably, the protective glide symmetries are well-preserved in the sonic-crystal realizations where higher-order topological transitions can be triggered by symmetry or geometry engineering.

Topological insulators are unconventional materials which host robust edge states and quantized transport or electromagnetic properties as dictated by the topological invariants of the occupied bulk bands [1, 2]. These topological invariants result from nontrivial quantization of Berry's phases arising from parallel transport in the Brillouin zone, which are essentially connected to dipole polarization and topological charge pumping in crystals [3]. Though developed for electronic systems, topological band theory also applies for photonic [4–16] and mechanical [17–27] waves, yielding rich phenomena and applications in various disciplines of science.

Recently, topological band theory was generalized from conventional (dipole) topology to quadrupole and octopole band topology [28–33], opening a pathway toward higher-order topology [34–46]. For instance, a 2D quadrupole topological insulator (QTI) has gapped edge states and topologically-protected corner states. QTI was proposed theoretically using a π -flux tight-binding model with noncommutative mirror symmetries [28, 29] and was later observed in mechanical [30] and microwave metamaterials [31], LC-circuits [32], and coupled optical waveguides [33]. However, the existing material realizations of QTIs often break the mirror symmetry that protects the quadrupole topology [30–32].

In this work, we present a theory of anomalous QTI (AQTI) in nonsymmorphic crystals without gauge flux. Using 2D square-lattice sonic crystals (SCs) as material realizations, we find that the AQTI is a topological state protected by two orthogonal glide symmetries. Due to these glide symmetries, the AQTI phase has several features that are distinct from the QTI model proposed in Refs. [28, 29]. These features include: (i) minimal four bands below the topological band gap which originates

from the band-sticking effect and the parity inversions, (ii) nondegenerate, gapped Wannier bands and special Wannier sectors with gapped composite Wannier bands, (iii) quantized Wannier band polarizations in the special Wannier sectors. Using SCs, we demonstrate that higher-order topological transitions can be triggered by symmetry or geometry engineering. We further present a full symmetry analysis for square and rectangular wallpaper crystals in the pursuit of quadrupole topology in flux-threading-free systems. Our discovery can be directly generalized to other classical-wave systems, e.g., photonic crystals, mechanical metacrystals. An experimental demonstration of the $p4gm$ SC as the acoustic AQTI has been demonstrated by some of us in Ref. [48] based on the theory in this work.

Nonsymmorphic $p4gm$ SCs.—We start with the AQTI phase in the $p4gm$ SCs [see Fig. 1(a)]. In each unit-cell, four identical arch-shaped epoxy blocks, with width w , height h and length l , serve as the scatterers for acoustic waves. The scatterers are arranged such that the SC has $p4gm$ nonsymmorphic symmetry group. The four key symmetries are: two orthogonal glide symmetries, $G_x = \{m_x|\tau_y\}$ and $G_y = \{m_y|\tau_x\}$ where $m_x := x \rightarrow \frac{a}{2} - x$, $m_y := y \rightarrow \frac{a}{2} - y$, $\tau_y := y \rightarrow y + \frac{a}{2}$ and $\tau_x := x \rightarrow x + \frac{a}{2}$ (a is the lattice constant, and the origin of the coordinate is at the center of the unit-cell), the inversion symmetry \mathcal{I} and the C_4 rotation symmetry.

The acoustic band structure, as obtained from COMSOL Multiphysics, is shown in Fig. 1(b). The band gap of concern is that between the fourth and the fifth bands. The dipole polarization of the bands below the

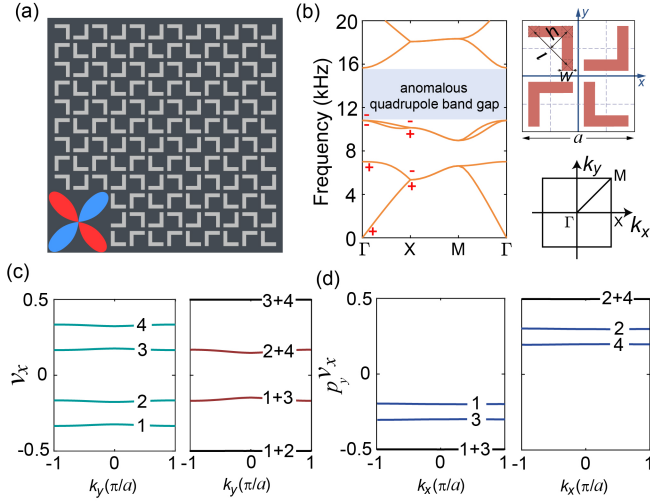


FIG. 1. (Color online) (a) A $p4gm$ SC that realizes the AQTI. Inset depicts the bulk quadrupole moment. (b) Acoustic band structure for $l = 0.42a$, $h = 0.21a$, $w = 0.1a$, and $a = 2$ cm. Symbols \pm label parities at the Γ and X points. Right panel: Unit-cell (brown shapes denote the epoxy scatterers, while dashed-lines depict the glide invariant lines) and Brillouin zone of the SC. (c) Wannier bands for the four acoustic bands below the gap (left), their combinations in the “1+3” and “2+4” Wannier sectors. Sound velocity and mass density of air are set as 343 m/s and 1.29 kg/m^3 , respectively.

gap is given by [29],

$$P_x = P_y = \frac{1}{4}(1 - \xi), \quad \xi = \prod_n \mathcal{I}_n(\Gamma)\mathcal{I}_n(X), \quad (1)$$

where $\mathcal{I}_n(\Gamma)$ and $\mathcal{I}_n(X)$ are the parity eigenvalues of the n^{th} -band ($n = 1, 2, 3, 4$) at the Γ and X points, respectively. From the parity eigenvalues in Fig. 1(b), the first and second (third and fourth) bands have a dipole polarization of $\vec{P} = (\frac{1}{2}, \frac{1}{2})$. Therefore, the band gap of concern has a vanishing dipole polarization, which is necessary for the emergence of the quadrupole topology [28].

The glide symmetries lead to the double degeneracy for all Bloch states on the XM and YM lines. This double degeneracy can be understood by constructing the anti-unitary operators $\Theta_j = G_j * \mathcal{T}$ ($j = x, y$) where \mathcal{T} is the time-reversal operator (i.e., complex conjugation). It is straightforward to obtain that $\Theta_y^2 \psi_{n,\vec{k}} = e^{ik_x a} \psi_{n,\vec{k}}$. Therefore, $\Theta_y^2 \psi_{n,\vec{k}} = -\psi_{n,\vec{k}}$ at the XM line, i.e., $k_x = \frac{\pi}{a}$. As an analog to the Kramers theorem for fermions, such a relation results in the double degeneracy for all Bloch states on the XM line [13]. According to the C_4 symmetry, the YM line has the same property.

The parity operator \mathcal{I} can be expressed using the glide operators, $\mathcal{I} = \tau_y^2 G_x G_y = \tau_x^2 G_y G_x$. Obviously, the two glide operators do not commute. Besides, we find that the double degeneracy at the X point consists of Bloch

states with opposite parities, since $\Theta_y \mathcal{I} = -\mathcal{I} \Theta_y$. This property constrains the parity-inversion between the Γ and X points and hence the dipole polarization. In this way, the quadrupole topology, since it requires a vanishing dipole polarization, emerge in our system when there are four bands below the band gap.

Wannier bands and nested Wannier bands.—The quadrupole topology is characterized by two features: (i) gapped Wannier bands for both ν_x and ν_y [28, 29]; (ii) quantized Wannier band polarizations. The second feature requires the mirror or glide reflection symmetry with respect to both x and y . The first condition, however, cannot be fulfilled in the presence of commutative mirror symmetries, as shown in Ref. [29].

The Wannier bands are calculated from the Wilson-loop approach [47]. For instance, $\exp[i2\pi\nu_x(k_y)]$, is obtained from the eigenvalues of the Wilson-loop operator $\hat{W}_{\vec{k}}^x = \mathcal{T}_P \exp[i\oint \hat{A}^x dk_x]$ where the superscript x and the subscript \vec{k} denote the direction and starting point of the Wilson-loop, respectively. \hat{A}^x is the non-Abelian (matrix) Berry connection for the first four bands. The matrix element is $A_{nm}^x = \langle u_n(\vec{k}) | i\partial_{k_x} | u_m(\vec{k}) \rangle$ for $n, m = 1, \dots, 4$. Here, $u_n(\vec{k})$ is the periodic part of the Bloch wavefunction, and \mathcal{T}_P is the path ordering operator. The results in Fig. 1(c) show that there are four nondegenerate, gapped Wannier bands.

The symmetry constraints on the Wannier bands are (see Supplemental Material for detailed derivations),

$$\nu_{x,n}(k_y) \stackrel{G_x}{=} -\nu_{x,n'}(k_y) + \frac{1}{2} \text{ mod } 1, \quad (2a)$$

$$\nu_{x,n}(k_y) \stackrel{G_y}{=} \nu_{x,n'}(-k_y) + \frac{1}{2} \text{ mod } 1, \quad (2b)$$

$$\nu_{x,n}(k_y) \stackrel{\mathcal{T}}{=} -\nu_{x,n'}(-k_y) \text{ mod } 1, \quad (2c)$$

$$\nu_{x,n}(k_y) \stackrel{\mathcal{T}}{=} \nu_{x,n}(-k_y) \text{ mod } 1. \quad (2d)$$

Here, $n' \neq n$ are Wannier band indices. We notice that \mathcal{I} transforms the first (second) Wannier band to the fourth (third) Wannier band. Besides, G_x transforms the first (third) Wannier band into the second (fourth) Wannier band, while G_y transforms the first (second) Wannier band to the third (fourth) Wannier band. Thus, the four Wannier bands are intrinsically connected to each other.

Following Refs. [28, 29], for the description of the quadrupole topology, it is important to introduce a division of the Wannier bands below and above $\nu_y = 0$. For the situations with more than two Wannier bands, such a division can have more possibilities. From the symmetry analysis above, we find that the division “1+2” and “3+4” always yield gapless composite Wannier bands, i.e., $\nu_{x,1} + \nu_{x,2} = \nu_{x,3} + \nu_{x,4} = \frac{1}{2} \text{ mod } 1$ [see Fig. 1(c)]. Only the division “1+3” and “2+4” leads to gapped composite Wannier bands (“gapped” meaning that the Wannier bands are away from the special values of 0 and $\pm\frac{1}{2}$) [see Fig. 1(c)]. We denote the Wannier sectors, “1+3”

and “2+4”, as I and II, respectively. The Wannier sector I (II) has a Wannier center below (above) the unit-cell center.

For Wannier sectors I and II, the Wannier band polarizations are calculated as $P_y^{\nu_x, I} = \frac{1}{2\pi} \int dk_x p_{y,1}^{\nu_x}(k_x) + p_{y,3}^{\nu_x}(k_x)$ and $P_y^{\nu_x, II} = \frac{1}{2\pi} \int dk_x p_{y,2}^{\nu_x}(k_x) + p_{y,4}^{\nu_x}(k_x)$, respectively. The nested Wannier bands, $p_{y,n}^{\nu_x}(k_x)$ ($n = 1, 2, 3, 4$), are calculated through the nested Wilson-loop approach (see Supplemental Material for details). The symmetry constraints on the Wannier band polarizations are (see Supplemental Material for proofs),

$$P_y^{\nu_x, I} \stackrel{G_x}{=} P_y^{\nu_x, II} \pmod{1}, \quad (3a)$$

$$P_y^{\nu_x, I} \stackrel{G_y}{=} -P_y^{\nu_x, I} \pmod{1}, \quad (3b)$$

The Wannier band polarizations is thus quantized as

$$P_y^{\nu_x, I} = P_y^{\nu_x, II} = 0, \frac{1}{2} \pmod{1}. \quad (4)$$

Similarly, the polarizations are quantized for the Wannier bands $\nu_y(k_x)$, leading to $P_x^{\nu_y, I} = P_x^{\nu_y, II} = 0, \frac{1}{2} \pmod{1}$. These constraints are confirmed by numerical calculations. In the $p4gm$ SC, $P_y^{\nu_x, I} = P_y^{\nu_x, II} = \frac{1}{2} \pmod{1}$ [see Fig. 1(d)], leading to nontrivial quadrupole topological index

$$q_{xy} = 2P_y^{\nu_x, I} P_x^{\nu_y, I} = \frac{1}{2} \pmod{1}. \quad (5)$$

Symmetry considerations.—The above results, in particular, the quantization of the bulk quadrupole moment q_{xy} is determined by the glide symmetries, G_x and G_y . Therefore, these results are also applicable to $p2gg$ SCs ($p2gg$ is similar to $p4gm$ but without the C_4 rotation symmetry), as shown in next section. We now consider possible emergence of the AQTI phase in square/rectangular groups within the 17 wallpaper groups. Fig. 2(a) illustrates the structures of four types of SCs with $p4gm$, $p2gg$, $p2mg$ and $p4mm$ symmetries, separately. Analysis on other symmetry groups are presented in the Supplemental Material. We remark that although we often use square-lattices as examples, the analysis can be directly generalized to rectangular lattices. For the sake of continuity, the $p2gg$ SC is constructed from the $p4gm$ SC by truncating the gray regions as depicted in the figure. The $p2mg$ SC has a glide symmetry, G_y , and a mirror symmetry, $M_x := (x, y) \rightarrow (-x, y)$. The $p4mm$ SC has two mirror symmetries, M_x and $M_y := (x, y) \rightarrow (x, -y)$. The unit-cells of the $p2mg$ and $p4mm$ SCs are doubled to enable comparison and analysis of the band structures and the Wannier bands for all SCs. The acoustic band structures for the $p2gg$ and $p4mm$ SCs are presented in Figs. 2(b) and 2(c), respectively. From the parity eigenvalues at the high-symmetry points of the Brillouin zone, we conclude that, for both SCs, the second band gap carries vanishing dipole polarization. However, the $p2gg$

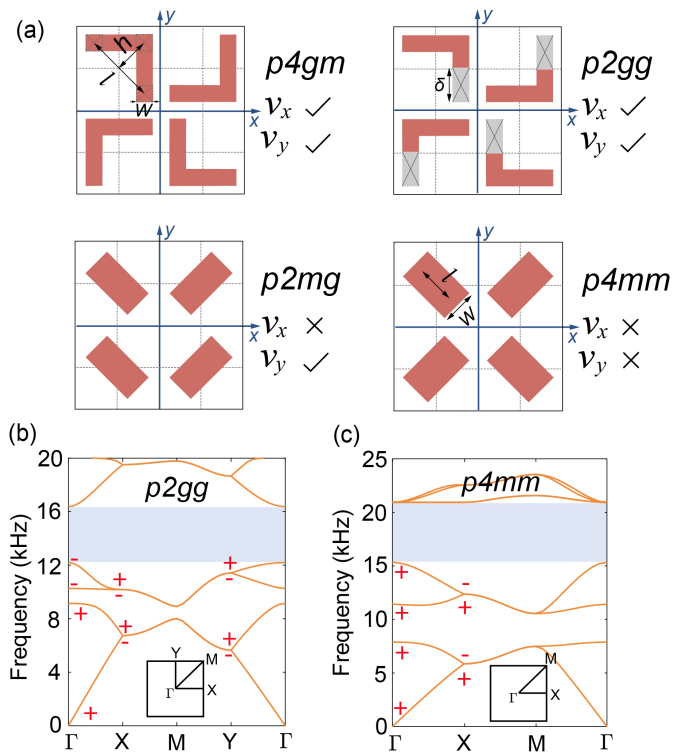


FIG. 2. (Color online) (a) Schematic of four types of SCs with $p4gm$, $p2gg$, $p2mg$ and $p4mm$ symmetries, separately. The brown shapes denote the epoxy scatterers, while the dashed-lines depict the glide invariant lines. We use the checkmarks to denote whether the Wannier bands ν_x and ν_y are gapped or not. (b)-(c) Acoustic band structures for the (b) $p2gg$ and (c) $p4mm$ SCs. The cyan regions denote the bulk band gaps of concern. Geometry parameters for (b): $l = 0.5a$, $h = 0.25a$, $w = 0.05a$, and $\delta = 0.1a$ (a is the lattice constant), and for (c): $l = 0.35a$, $h = 0$, and $w = 0.25a$. Here, the $p2gg$ SC is derived from the $p4gm$ SC by removing the gray regions of length δ for the epoxy scatterers [see figure (a)].

SCs can have nontrivial quadrupole topology, whereas the $p4mm$ SCs cannot. The underlying reason is that the commutative mirror symmetries, M_x and M_y , in the $p4mm$ SCs lead to degenerate Wannier bands and gapless composite Wannier bands. Similar results were found in the $p2mm$ and $c2mm$ wallpaper crystals. A special case is $p2mg$ crystals where the commutation between the mirror and glide symmetry at special high-symmetry points yields gapped Wannier bands for ν_y , but gapless Wannier bands for ν_x . These wallpaper crystals cannot support quadrupole topology. We find that to have nondegenerate, gapped Wannier bands, both glide symmetries G_x and G_y are needed, or if the system has neither glide nor mirror symmetry in the x and/or y direction. In the latter case (including $p2ll$, $p1ml$, $p1gl$, $c1ml$, $p4$ wallpaper crystals), however, the Wannier band polarizations are not quantized (at least for one of them, ν_x or ν_y), because the quantization of the Wannier band polarizations

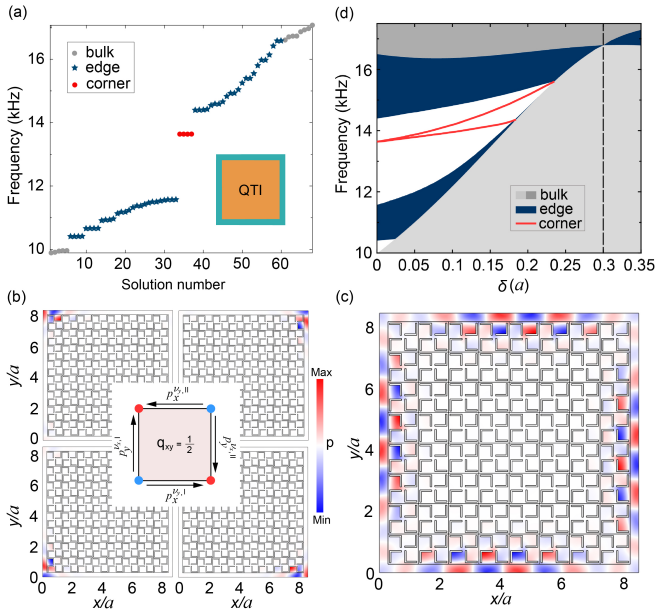


FIG. 3. (Color online) (a) Eigenstates spectrum for a square-shaped finite-sized $p4gm$ SC with hard-wall boundary conditions, showing the coexistence of the bulk, edge and corner states. (b)-(c): Acoustic wavefunction (the acoustic pressure field p) for the (b) corner and (c) edge states. (d) Evolution of the bulk, edge and corner spectra with the truncation length δ for the $p2gg$ SC. The topological band gap is tuned to close and reopen with increasing δ . Bulk band gap closing at $\delta = 0.3a$ is indicated by the dashed line.

are dictated by the glide or mirror symmetry. Therefore, only for the $p4gm$ and $p2gg$ SCs, the AQTI phase can emerge.

Edge and corner states.—The nontrivial quadrupole topology leads to gapped edge states and in-gap corner states. To demonstrate these topological boundary states, we study a finite SC with 8×8 unit-cells cladded by hard-wall boundaries. A finite-width ($0.28a$) air channel is introduced between the hard-wall boundaries and the SC to tune the edge band gap to the middle of the bulk band gap. Such a narrow air channel cannot introduce waveguide modes in the bulk band gap, since the waveguide modes can appear only at much higher frequencies (> 30 kHz). In accordance with our theory, the calculated spectrum [see Fig. 3(a)] shows the emergence of four corner states in the common spectral gap of the edge and bulk. The acoustic wavefunctions of the corner and edge states are shown in Figs. 3(b) and 3(c), respectively. The four degenerate corner states exhibit the quadrupole symmetry.

Geometry engineering in the $p2gg$ group.—Fig. 3(d) presents the evolution of the bulk, edge and corner states as a function of the geometry parameter δ . For $\delta = 0$, the SC has C_4 symmetry and belongs to the $p4gm$ group where all four corner states are degenerate. As δ in-

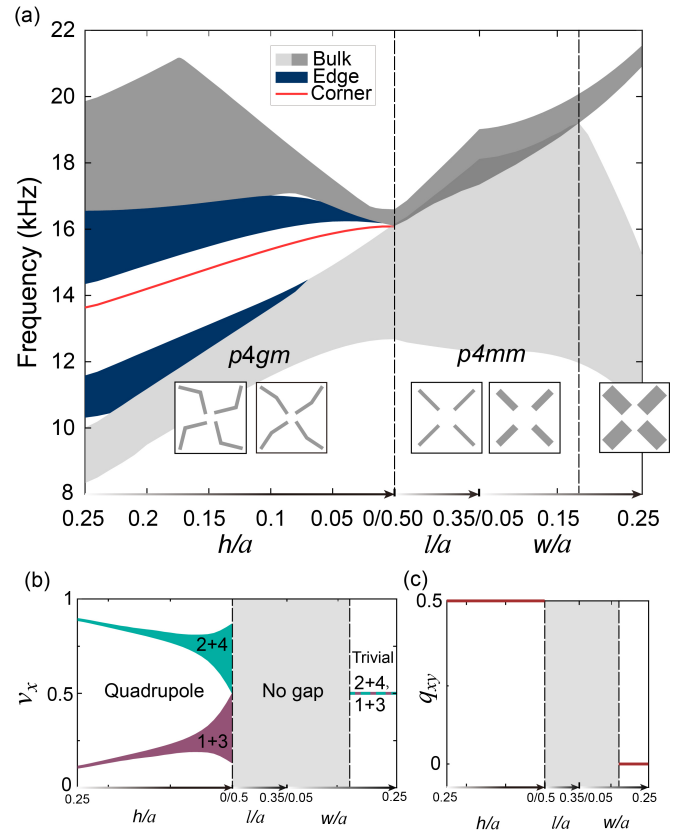


FIG. 4. (Color online) (a) Evolution of the bulk, edge and corner spectra during a geometry transformation from the $p4gm$ group to the $p4mm$ group: The starting point has $l = 0.5a$, $h = 0.25a$, and $w = 0.05a$. First, h goes from $0.25a$ to 0 . Then, l goes from $0.5a$ to $0.35a$. Finally, w goes from $0.05a$ to $0.25a$. The vertical dashed lines indicate the conditions where the bulk band gap closes or opens. The left, middle and right regions separated by the dashed lines correspond to the QTI phase, the gapless phase, and the trivial phase, separately. Several representative unit-cell geometries are illustrated as the insets. (b)-(c) Evolution of the Wannier bands (b) and the quadrupole topological index q_{xy} (c) during the geometry transformation process.

creases, the degeneracy is lifted and split into two doublets: the left-upper and right-lower corner states form a doublet, while the right-upper and left-lower corner states form another doublet. At large δ , the edge band gap is closed ($\delta = 0.233a$), while the corner states merge into the edge, i.e., their wavefunctions gradually transform from fully localized to extensive along the edges. The closure of the edge band gap signals the transition into a quadrupole trivial phase. Further increase of δ leads to bulk band gap closing at $\delta = 0.3a$ where the edge states merge into the bulk (see Supplemental Material for details).

Symmetry engineering.—Starting from the $p4gm$ SC, one can keep the C_4 symmetry and gradually transform into the $p4mm$ SC, by reducing the geometry parameter

h. We study a continuous transformation process with first (i) h going from $0.25a$ to 0 , and then (ii) l going from $0.5a$ to $0.35a$, and lastly (iii) w going from $0.05a$ to $0.25a$. The phase diagram for the corner, edge and bulk spectra are shown in Fig. 4(a) which indicates a topological transition taking place exactly at the geometry transition point, i.e., $h = 0$. While the SC is transformed from the $p4gm$ group to the $p4mm$ group, the bulk band gap closes and the corner states merge into the bulk. The edge states remain gapped and gradually merge into the bulk bands before the bulk band gap closing. The bulk band gap remains closed in stage (ii). When the band gap is reopened in stage (iii), the corner states disappear in the bulk band gap. The phase diagram in Fig. 4(a) thus manifests directly the bulk-corner correspondence due to the quadrupole topology.

Such a topological transition is also manifested in the Wannier bands. As shown in Fig. 4(b), the Wannier band gap for the “1+3” and “2+4” sectors is closed when the SC experiences the symmetry transition from the $p4gm$ group to the $p4mm$ group. We find that the $p4gm$ SCs have nontrivial quadrupole topology, i.e., $q_{xy} = \frac{1}{2}$ (see Fig. 4(c); This is confirmed in a recent experiment [48]). In contrast, when the band gap is reopened in the $p4mm$ SC, the Wannier bands are degenerate which cannot support the quadrupole topology.

Finally, we remark that the acoustic topological band gaps studied here do not have the chiral symmetry. Consequently, the corner states are not fixed at the mid-gap frequency. However, as shown in Ref. [49], this property can be used to move the corner states into the bulk continuum where the corner states still survive.

Note added: At the final stage of this work, we became aware of recent works on boundary obstructed topological phases [50] (including some quadrupole topological insulators) and quadrupole topological insulators in magnetized systems [51, 52].

Acknowledgments.— J.H.J, Z.K.L, H.X.W, and Z.X acknowledge supports from the Jiangsu specially-appointed professor funding and the National Natural Science Foundation of China (Grant No. 11675116). M.H.L thanks the support from the National Key R&D Program of China (2017YFA0303702 and 2018YFA0306200). J.H.J thanks Prof. Gil Young Cho for illuminating discussions.

* Corresponding author: jianhuajiang@suda.edu.cn

[1] M. Z. Hasan and C. L. Kane, “Colloquium: Topological insulators”, *Rev. Mod. Phys.* **82**, 3045-3067 (2010)
 [2] X. L. Qi and S.-C. Zhang, “Topological insulators and superconductors”, *Rev. Mod. Phys.* **83**, 1057-1110 (2011).
 [3] D. Vanderbilt and R. D. King-Smith, “Electric polarization as a bulk quantity and its relation to surface charge”, *Phys. Rev. B* **48**, 4442-4455 (1993).

[4] F. D. M. Haldane and S. Raghu, “Possible realization of directional optical waveguides in photonic crystals with broken time-reversal symmetry”, *Phys. Rev. Lett.* **100**, 013904 (2008).
 [5] Z. Wang, Y. Chong, J. D. Joannopoulos, and M. Soljačić, “Observation of unidirectional backscattering immune topological electromagnetic states”, *Nature* **461**, 772-775 (2009).
 [6] L. Lu, L. Fu, J. D. Joannopoulos, and M. Soljačić, “Weyl points and line nodes in gyroid photonic crystals”, *Nat. Photon.* **7**, 294-299 (2013).
 [7] M. Hafezi, S. Mittal, J. Fan, A. Migdall, and J. M. Taylor, “Imaging topological edge states in silicon photonics”, *Nat. Photon.* **7**, 1001-1005 (2013).
 [8] M. C. Rechtsman *et al.*, “Photonic Floquet topological insulators”, *Nature* **496**, 196-200 (2013).
 [9] A. B. Khanikaev *et al.*, “Photonic topological insulators”, *Nat. Mater.* **12**, 233-239 (2013).
 [10] W.-J. Chen *et al.*, “Experimental realization of photonic topological insulator in a uniaxial metacrystal waveguide”, *Nat. Commun.* **5**, 6782 (2014).
 [11] L.-H. Wu and X. Hu, “Scheme for achieving a topological photonic crystal by using dielectric material”, *Phys. Rev. Lett.* **114**, 223901 (2015).
 [12] L. Xu, H.-X. Wang, Y.-D. Xu, H.-Y. Chen, and J.-H. Jiang, “Accidental degeneracy and topological phase transitions in two-dimensional core-shell dielectric photonic crystals”, *Opt. Express* **24**, 18059-18071 (2016).
 [13] H.-X. Wang, Y. Chen, Z. H. Hang, H.-Y. Kee, and J.-H. Jiang, “Type-II Dirac photons”, *npj Quantum Materials* **2**, 54 (2017).
 [14] M. Verbin, O. Zilberberg, Y. E. Kraus, Y. Lahini, and Y. Silberberg, “Observation of Topological Phase Transitions in Photonic Quasicrystals”, *Phys. Rev. Lett.* **110**, 076403 (2013).
 [15] O. Zilberberg *et al.*, “Photonic topological boundary pumping as a probe of 4D quantum Hall physics”, *Nature* **553**, 59-62 (2018).
 [16] L. Lu, J. D. Joannopoulos, and M. Soljačić, “Topological photonics”, *Nat. Photon.* **8**, 821-829 (2014).
 [17] Z. G. Chen *et al.*, “Accidental degeneracy of double Dirac cones in a phononic crystal”, *Sci. Rep.* **4**, 4613 (2014).
 [18] Z. J. Yang, F. Gao, X. H. Shi, X. Lin, Z. Gao, Y. D. Chong, and B. Zhang, “Topological acoustics”, *Phys. Rev. Lett.* **114**, 114301 (2015).
 [19] X. Ni *et al.*, “Topologically protected one-way edge mode in networks of acoustic resonators with circulating air flow”, *New J. Phys.* **17**, 053016 (2015).
 [20] M. Xiao *et al.*, “Geometric phase and band inversion in periodic acoustic systems”, *Nat. Phys.* **11**, 240-244 (2015).
 [21] C. He *et al.*, “Acoustic topological insulator and robust one-way sound transport”, *Nat. Phys.* **12**, 1124-1129 (2016).
 [22] J. Lu, C. Qiu, L. Ye, X. Fan, M. Ke, F. Zhang, and Z. Liu, “Observation of topological valley transport of sound in SCs”, *Nat. Phys.* **13**, 369-374 (2017).
 [23] M. Xiao, W. J. Chen, W. Y. He, and C. T. Chan, “Synthetic gauge flux and Weyl points in acoustic systems”, *Nat. Phys.* **11**, 920-924 (2015).
 [24] F. Li *et al.*, “Weyl points and Fermi arcs in a chiral phononic crystal”, *Nat. Phys.* **14**, 30-34 (2017).
 [25] H. He *et al.*, “Topological negative refraction of surface acoustic waves in a Weyl phononic crystal”, *Nature* **560**,

- 61-64 (2018).
- [26] R. Süssstrunk and S. D. Huber, “Observation of phononic helical edge states in a mechanical topological insulator”, *Science* **349**, 47-50 (2015).
- [27] L. M. Nash *et al.*, “Topological mechanics of gyroscopic metamaterials”, *Proc. Natl Acad. Sci. USA* **112**, 14495-14500 (2015).
- [28] W. A. Benalcazar, B. A. Bernevig, and T. L. Hughes, “Quantized electric multipole insulators”, *Science* **357**, 61-66 (2017).
- [29] W. A. Benalcazar, B. A. Bernevig, and T. L. Hughes, “Electric multipole moments, topological multipole moment pumping, and chiral hinge states in crystalline insulators”, *Phys. Rev. B* **96**, 245115 (2017).
- [30] M. Serra-Garcia *et al.*, “Observation of a phononic QTI”, *Nature* **555**, 342-345 (2018).
- [31] C. W. Peterson, W. A. Benalcazar, T. L. Hughes, and G. Bahl, “A quantized microwave quadrupole insulator with topological protected corner states”, *Nature* **555**, 346-350 (2018).
- [32] S. Imhof *et al.*, “Topoelectrical circuit realization of topological corner modes”, *Nat. Phys.* **14**, 925-929 (2018).
- [33] S. Mittal, V. V. Orre, G. Zhu, M. A. Gorlach, A. Poddubny, and M. Hafezi, “Photonic quadrupole topological phases”, *Nat. Photon.* **13**, 692-696 (2019).
- [34] F. Schindler *et al.*, “Higher-order topological insulators”, *Sci. Adv.* **4**, eaat0346 (2018).
- [35] J. Langbehn, Y. Peng, L. Trifunovic, F. von Oppen, and P. W. Brouwer, “Reflection-symmetric second-order topological insulators and superconductors”, *Phys. Rev. Lett.* **119**, 246401 (2017).
- [36] Z. D. Song, Z. Fang, and C. Fang, “ $(d-2)$ -dimensional edge states of rotation symmetry protected topological states”, *Phys. Rev. Lett.* **119**, 246402 (2017).
- [37] M. Ezawa, “Higher-order topological insulators and semimetals on the breathing Kagome and pyrochlore lattices”, *Phys. Rev. Lett.* **120**, 026801 (2018).
- [38] B. Y. Xie *et al.*, “Second-order photonic topological insulator with corner states”, *Phys. Rev. B* **98**, 205147 (2018).
- [39] J. Noh *et al.*, “Topological protection of photonic mid-gap defect modes”, *Nat. Photon.* **12**, 408-415 (2018).
- [40] H. Xue, Y. Yang, F. Gao, Y. Chong, and B. Zhang, “Acoustic higher-order topological insulator on a kagome lattice”, *Nat. Mater.* **18**, 108-112 (2019).
- [41] X. Ni, M. Weiner, A. Alú, and A. B. Khanikaev, “Observation of higher-order topological acoustic states protected by generalized chiral symmetry”, *Nat. Mater.* **18**, 113-120 (2019).
- [42] X. Zhang *et al.*, “Second-order topology and multi-dimensional topological transitions in sonic crystals”, *Nat. Phys.* **15**, 582-588 (2019).
- [43] A. E. Hassan, F. K. Kunst, A. Moritz, G. Andler, E. J. Bergholtz, and M. Bourennane, “Corner states of light in photonic waveguides”, *Nat. Photon.* **13**, 697-700 (2019).
- [44] X.-D. Chen *et al.*, “Direct observation of corner states in second-order topological photonic crystal slabs”, *Phys. Rev. Lett.* **122**, 233902 (2019).
- [45] B.-Y. Xie *et al.*, “Visualization of higher-order topological insulating phases in two-dimensional dielectric photonic crystals”, *Phys. Rev. Lett.* **122**, 233903 (2019).
- [46] S. Franca, J. van den Brink, and I. C. Fulga, “An anomalous higher-order topological insulator”, *Phys. Rev. B* **98**, 201114(R) (2018).
- [47] H.-X. Wang, G.-Y. Guo, and J.-H. Jiang, “Band topology in classical waves: Wilson-loop approach to topological numbers and fragile topology”, *New J. Phys.* **21**, 093029 (2019).
- [48] X. Zhang *et al.*, “Symmetry-protected hierarchy of anomalous multipole topological band gaps in nonsymorphic metacrystals”, *Nat. Commun.* **11**, 65 (2020).
- [49] W. A. Benalcazar and A. Cerjan, “Bound states in the continuum of higher-order topological insulators”, *Phys. Rev. B* **101**, 161116(R) (2020).
- [50] E. Khalaf, W. A. Benalcazar, T. L. Hughes, and R. Queiroz, “Boundary-obstructed topological phases”, arXiv:1908.00011
- [51] B. J. Wieder, Z. Wang, J. Cano, X. Dai, L. M. Schoop, B. Bradlyn, and B. A. Bernevig, “Strong and ‘fragile’ topological Dirac semimetals with higher-order Fermi arcs”, Preprint at <https://abs.arXiv.org/1908.00016>.
- [52] L. He, Z. Addison, E. J. Mele, and B. Zhen, “Quadrupole topological photonic crystals”, Preprint at <https://abs.arxiv.org/1911.03980>.